RESEARCH PAPER

Experimental Investigation on Bonded and Screwed Carbon Fiber-Reinforced Plastic Plates on Timber Column–Sill Joints

Rintaro Ueda[1] · Akio Sakamoto[2] · Kei Sawata[3] · Yoshihisa Sasaki[3] · Takanobu Sasaki[3]

Abstract

In this study, timber column–sill joints strengthened with carbon fiber-reinforced plastic (CFRP) plates using bonds and screws were subjected to loading tests. Twelve joint specifications were considered depending on different combinations of the CFRP plate surface finish and thickness and the type of bond, and the corresponding effects on the load–displacement behavior of the joints were investigated. Three failure modes were observed in addition to the peeling of the CFRP plate. The specimens that failed owing to screw tear out and screw head pull-through in the CFRP plate or splitting of the sill showed load–displacement curves of a similar shape. Those that failed owing to buckling of the CFRP plate showed a rapid and substantial load decrease due to failure. This failure mode was only observed in 0.50 mm thick CFRP plate specimens. When a peel-ply CFRP plate was installed in the column–sill joint specimens, similar secant stiffnesses were observed in the silicon and epoxy resin-bonded specimens, both with high shear strength. Although the specimens with bonds with a high shear strength showed lower deformation performance, the specimens' maximum load increased with the bond's shear strength. The maximum load improved for a 0.75 mm thick peel-ply silicon- or epoxy-bonded CFRP plate. The load's maximum value after peeling the CFRP plate was 0.79–1.23 times as large as the maximum load of the no-bond specimens and did not change significantly.

Keywords Column–sill joint · Bond type · Failure mode · Stiffness · Maximum load

List of symbols

$P_{S\text{-max}}$ Maximum load of the no-bond specimens
P_r Maximum load after peeling of the CFRP plate
D_u Displacement corresponding to the value of $0.8 \times P_{S\text{-max}}$

1 Introduction

Recently, carbon-fiber-reinforced plastics (CFRPs) have been increasingly used in construction. Numerous studies have reported on strengthening structures using CFRP sheets and plates for concrete construction. CFRP materials are usually externally installed by bonds, and the guidelines for strengthening reinforced concrete structures using FRP have been published in countries such as Japan [1], America [2], and Italy [3].

Several experimental [4–6] and theoretical [7, 8] studies on FRP bonded to concrete joints have been conducted in the last two decades [9]. Based on the knowledge and experience acquired in concrete construction, CFRP has been applied to strengthen timber structures. This technique is less intrusive than are the other techniques, and it allows the preservation of the original appearance of the target construction and can be performed rapidly [10]. In Italy, guidelines for the design and construction of externally bonded FRP systems for strengthening existing timber structures have been established and published [11]. However, more studies have focused on the application of CFRP materials to concrete construction than timber structures.

Timber structures are often strengthened by installing CFRP materials with bonds or fasteners. The interfacial behavior of CFRPs bonded to timber joints has been

✉ Kei Sawata
   ksawata@for.agr.hokudai.ac.jp

[1]   Gifu Academy of Forest Science and Culture, 88 Sodai, Mino, Gifu 501-3714, Japan

[2]   Design and Innovation Co., Ltd., 5-24-14 Kamiikedai, Ota-ku, Tokyo 145-0064, Japan

[3]   Research Faculty of Agriculture, Hokkaido University, N9 W9, Sapporo, Hokkaido 060-8589, Japan

investigated, and analytical models have been developed [9, 10, 12–17]. Wan et al. [12] developed an exponential bond strength model from 86 single-shear tests of FRP–timber joints with six adhesive types, two FRP plate types, and two wood species. They concluded that the difference in adhesive type did not noticeably affect the bond stress–slip response. All the adhesives used in the study were epoxy based, and their individual differences were not mentioned. Biscala and Diogo [10] conducted single-shear tests on FRP-to-timber bonded joints with additional mechanical anchorage to prevent the premature debonding of FRP strips from the timber surface. The study reported that most of the adapted mechanical anchorages increased the load capacities of the joints compared to those without mechanical anchorages. Some studies have focused on strengthening timber beams with CFRP strips or sheets, mainly bonded externally to the tension side [18–23]. Schober et al. [18] studied the bending strength of old timber beams strengthened with CFRP strips bonded externally or in slot to the tension zone and reported that the presence of CFRP strengthening arrested the crack opening, and the strengthened beams exhibited more ductile behavior. Garcia et al. [19] studied the strength properties of timber beams strengthened with externally bonded U-shaped basalt fibers and unidirectional and bidirectional CFRP fabrics on the tension side. They reported that the beams with strengthening exhibited greater stiffness irrespective of the used fiber fabrics than those without strengthening. Using bidirectional CFRP fabrics offered better results than unidirectional fabrics, even with lower grammages than the latter. This result implies the potential cost-effectiveness of using bidirectional CFRP materials for strengthening timber structures. Biscaia et al. [22] compared flexural-strengthened old timber beams with externally bonded CFRP strips on the tension side. They reported that the slips between the CFRP and timber and bond stresses within the CFRP-to-timber interface were reduced.

The installation methods for FRP with metal fasteners are described in the guidelines [11]. Righetti et al. [24] investigated the bending behavior of timber beams strengthened with CFRP plates screwed on the tension side. They reported that the strengthening increased bending strength by 29.4% and global modulus of elasticity by 68.4%. The typical failure mode was timber cracking in the tension zone with no failure of the CFRP plates. Additionally, Righetti et al. [25] studied the shear resistance and deformation characteristics of single-screwed joints using FRP plates. They reported that the failure of the specimens was mainly due to screw yielding at the timber and FRP plates, and slippage between the plate and wood was observed. Studies have been conducted on CFRP to timber joints with bonds or fasteners; however, few reports on the

load-deformation behavior of combined joints with bonds and fasteners are available.

When wooden houses are subjected to horizontal forces, such as earthquakes and wind, an uplift force occurs in the column–sill timber joints. In recent years, metal hardware has often been installed in the column–sill joints of wooden houses to resist this uplift force; however, this is not often performed in older wooden houses. When metal hardware is installed in timber, probable condensation on the metal hardware can increase the moisture content of the timber. The increased moisture content at the sill often causes biodegradation of timber. Given that the CFRP plates are less likely to condense than metal hardware, the external installation of CFRP plates can be an appropriate method for strengthening column–sill joints in such houses. Therefore, cyclic loading tests were conducted on column–sill joints strengthened with CFRP plates installed using both bonds and screws. The effects of the CFRP specifications and bond type on the load–displacement behavior of these joints were investigated.

2 Experimental Details

2.1 Materials

2.1.1 CFRP Plates

The design of the CFRP plate is illustrated in Fig. 1. The plates were 105 mm wide and 210-mm long and had 20×6.0 mm diameter holes (as shown) for the screws. The plates were either 0.50- or 0.75 mm thick. The plate specifications are listed in Table 1. The plates comprised two or three layers of laminated F6343B-05P prepreg sheets. Each layer was 0.24 mm thick and had a fiber areal weight of 200 g/m^2. The prepreg sheets were composed of
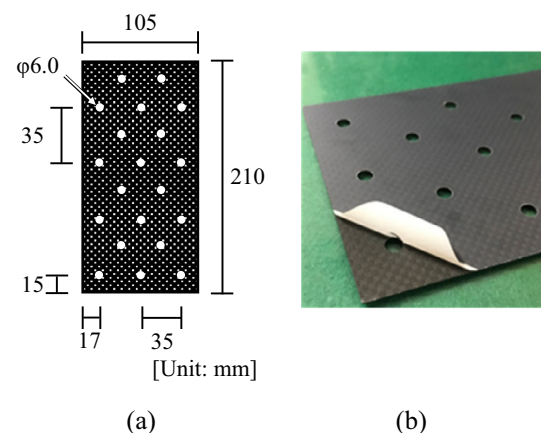

Fig. 1 CFRP plate: **a** Geometrical dimensions; **b** CFRP plate with a peel ply

Table 1 Details of CFRP

CFRP type	Number of laminates	Thickness of CFRP plate (mm)	Surface of CFRP plate
50S	2	0.50	Sanding
50P	2	0.50	Removal of a peel ply
75P	3	0.75	Removal of a peel ply

plain weave T300-3 K carbon fiber manufactured by Toray Industries Inc. (Tokyo) and comprised carbon fibers arranged in two orthogonal directions. The tensile strength of the carbon fibers was 3530 MPa. The matrix resin was an epoxy resin.

Peel plies are often used in composite manufacturing to create clean and rough surfaces for bonding [26, 27]. Mold release agents often remain on the surface of molded CFRPs, affecting the bonding properties between the CFRP and timber. To remove these remnants, CFRP plates with two different surfaces were used. One had a polyester peel ply on the surface of the CFRP (Fig. 1b), which was removed prior to the bonding. The other surface type was sanded with sandpaper on the surface of the CFRP without a peel ply to roughen the surface for bonding. The abrasive grain size of the sandpaper was 80–106 μm, and the mold-releasing agent was removed by sanding. The sanded 0.50 mm thick, peel ply 0.50 mm thick, and peel ply 0.75 mm thick CFRP plates were named 50S, 50P, and 75P, respectively. The timber surface was not sanded.

2.1.2 Columns and Sills

The design of the columns and sills is illustrated in Fig. 2. The columns (105 mm × 105 mm × 645 mm) and sills (105 mm × 105 mm × 1000 mm) were prepared from Japanese cedar (*Cryptomeria japonica*). The mean wood density was 373 kg/m^3, and the dimensions of the tenons and mortises were 75 mm × 30 mm × 45 mm and 78 mm × 33 mm × 50 mm, respectively. The dimensions of the tenons were smaller than those of the mortises to avoid friction between the tenons and mortises when investigating the load–displacement behavior of the bonded and screwed joints.

2.2 Column–Sill Joint Specimens

The CFRP plate was installed on one side of the column and sill members. Four approaches can be adopted to join CFRP plates to members. One was a screwed joint without a bond (no-bond). The others were joints with screws and
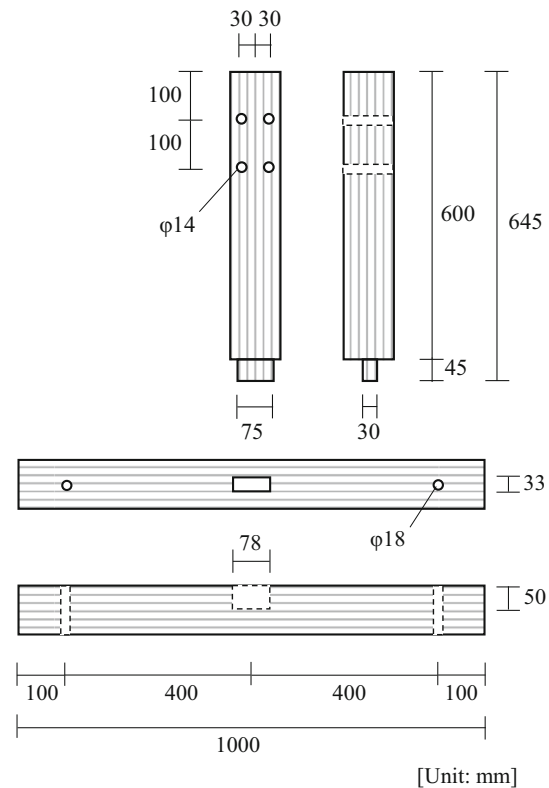

Fig. 2 Geometrical dimensions of column and sill

bonds combined. The screw design is shown in Fig. 3. The screws used in this study were 41 mm long with a 31 mm long shank; the outer thread and core diameters were 4.0 mm and 2.65 mm, respectively. These screws were manufactured by Synegic Co., Ltd. (Miyagi) for timber structures, and the yield strength of the screws was 1553 MPa. The yield strength was determined from a four-point bending test with support and load spans of 27 mm and 6 mm, respectively. The CFRP plate was fastened to the column and sill using ten screws in each.

The following three types of bonds were prepared: two silicon resin adhesives (Silicon A and B) and one epoxy resin adhesive (Epoxy). The bond specifications are listed in Table 2. Epoxy resin adhesives are used post-strengthening timber structures; however, they might be generally too rigid for bonded timber joints [18]. The silicon resin
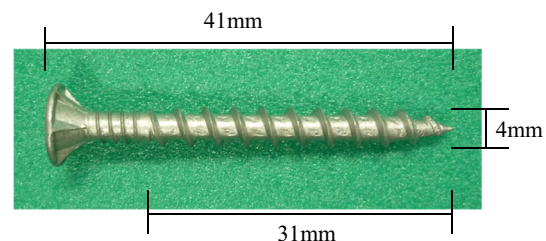

Fig. 3 Dimension of screw

Table 2 Details of bond type

Type	Bond	f_s (MPa)
Silicon A	Silicon resin	0.76
Silicon B	Silicon resin	5.62
Epoxy	Epoxy resin	18.9

f_s: shear strength

adhesives used in this study were elastic curing adhesives and might be able to increase displacement during shear deformation of bonded joints. Therefore, three different bonds were provided to investigate the effects of the shear strength of bonds on the strength properties of column–sill joints with CFRP plates installed using both bonds and screws. The shear strengths of the bonds are listed in Table 2. The shear strengths were determined from single-lap shear tests according to JIS K 6850, equivalent to ASTM D 1002 and ISO 4587. The shear strengths of Silicon A, Silicon B, and Epoxy were 0.76, 5.62, and 18.9 MPa, respectively. The specimens with the adhesive applied were placed at room temperature and humidity during curing. Twelve specifications of column–sill joint specimens comprising three different CFRP plates with four different joint types were considered, and tests were conducted on three specimens per specification.

2.3 Experimental Methods

The test setup is shown in Fig. 4. The column was fastened to a steel jig using four bolts with a diameter of 12 mm. The sill was fastened to a steel frame using two bolts with a diameter of 16 mm. The fastening position was 400 mm from the center of the column.

The displacement between the column and sill was the mean value recorded by the two displacement transducers
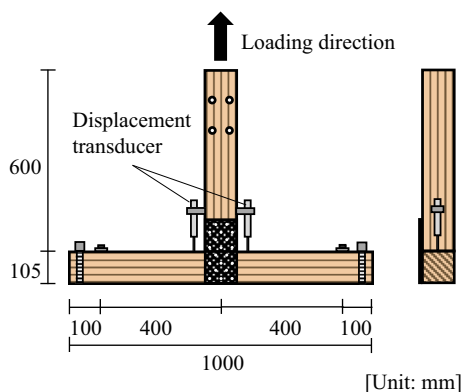

Fig. 4 Outline of column–sill joint specimen with CFRP

located on each side of the column. Cyclic tests were conducted using a computer-controlled hydraulic-actuated testing machine. The load was applied to produce a $0.5 \times$ yield displacement, which was subsequently reduced to 0 mm. This loading procedure was repeated to produce displacements of 1.0, 2.0, 4.0, 6.0, and $8.0 \times$ yield displacement; subsequently, the load was monotonically applied. The tests were terminated when the load dropped below 50% of the maximum load [28]. The yield displacement was obtained from the preliminary monotonic loading test of the column–sill joint specimens with a 0.75 mm thick CFRP plate. The yield displacements of specimens with no-bond, Silicon A, Silicon B, and Epoxy were 1.0, 1.6, 0.8, and 1.5 mm, respectively.

3 Results and Discussion

3.1 Failure of Column–Sill Joint Specimens

The column–sill joint specimens with bonds and screws initially failed at the bonded joint between the CFRP plate and timber, and the CFRP plate was peeled off from one or both columns and sills. The subsequent failures of the column–sill joint specimens can be classified into three modes: (a) screw tear out and screw head pull-through in the CFRP plate; (b) splitting of the sill; and (c) buckling of the CFRP plate; as shown in Fig. 5. A diagram of the progress of the screw tear and screw head pull-through is shown in Fig. 6. The screw joints resisted external forces after the bonded joint failed. The embedment of the CFRP plate by the screws increased with the deformation of the column–sill joint specimen. Finally, the specimen failed with a screw tear out and screw head pull-through. The occurrence rates of the failure modes are shown in Fig. 7. Tear out and screw head pull-through were frequently observed in the 50S and 50P CFRP plate specimens. For the 75P CFRP plate, this failure occurred in the no-bond and Silicon A specimens.

A split of the sill was observed in some column–sill joint specimens with the 50P CFRP plate bonded with Silicon B and Epoxy, but occurred mostly on the 75P CFRP plate specimens. When the embedding load of the CFRP plate was high and the CFRP plate was rigidly fastened to the sill, sill splitting occurred mainly on the upper edge (Fig. 5) owing to the small edge distance. As shown in Fig. 8, some specimens exhibited a split near the center of the sill, and the crack length associated with such splits was larger than that of the splits near the edge of the sill.

The embedded marks exhibited slit-like shapes when the screw was embedded in the CFRP plate. If the screw passed through the embedding marks under a reversed
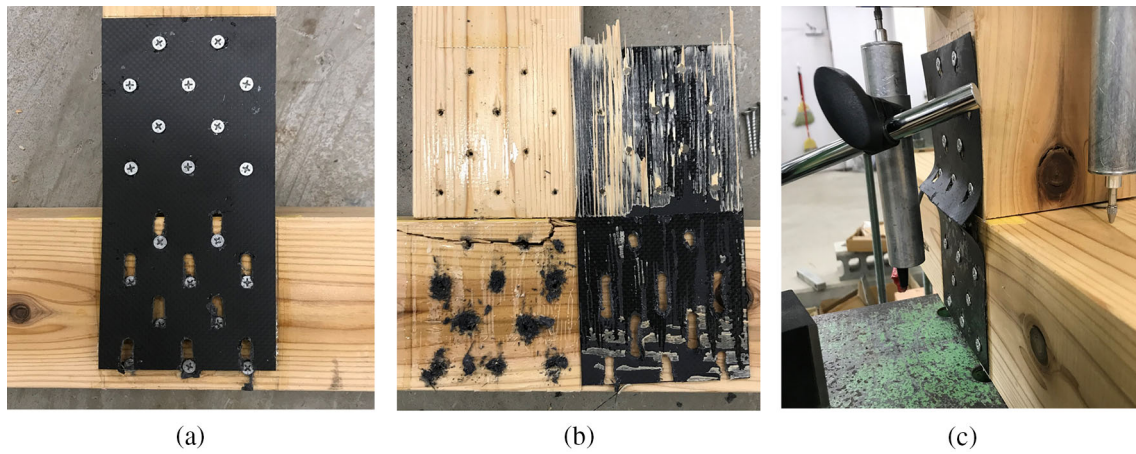
Fig. 5 Failure mode of column–sill joint specimen: **a** tear out and screw head pull-through (50S CFRP plate specimen bonded with Silicon B); **b** split of sill (75P CFRP plate specimen bonded with Silicon B); **c** buckling of CFRP plate (50P CFRP plate specimen bonded with Silicon B)
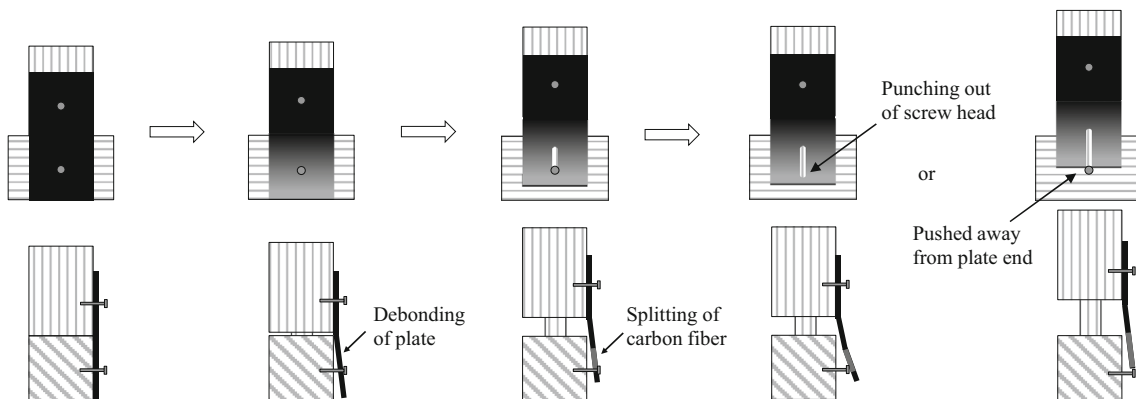

Fig. 6 Deformation process of screw tear out and screw head pull-through
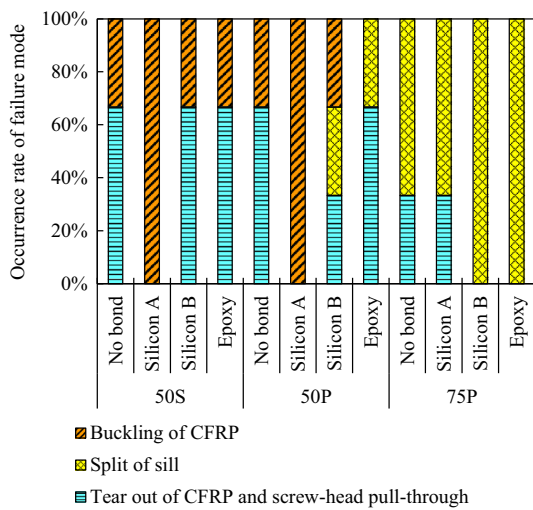

Fig. 7 Occurrence rate of failure mode of column–sill joint specimens

Fig. 8 Split of sill from center

50P CFRP plate column–sill joint specimens. When the CFRP plate was thin, buckling occurred under reversed loading.

load, it returned to the original screw hole. Otherwise, the CFRP plate failed by buckling, as shown in Fig. 9. Buckling of the CFRP plate was observed only in the 50S and
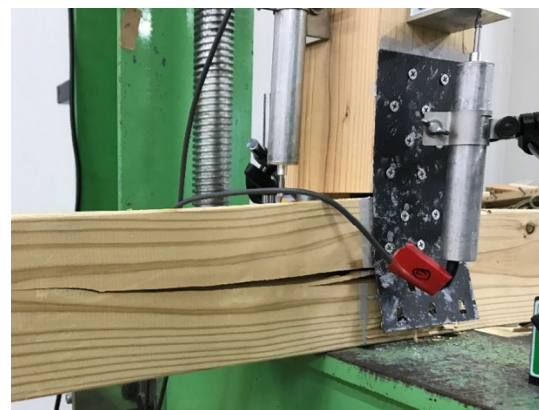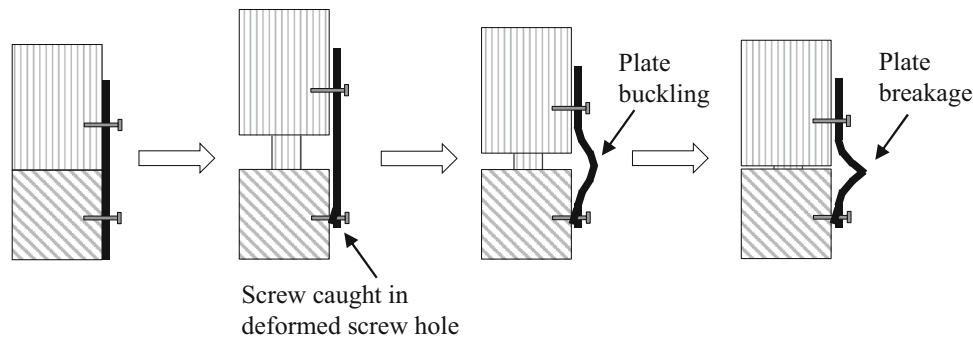
Fig. 9 Buckling process of CFRP plate

3.2 Load–Displacement Behavior

Envelope load–displacement curves were obtained for the column–sill joint specimens from the cyclic load–displacement curves, as shown in Fig. 10. The load of the no-bond specimens showed a linear increase up to the yield point and a continuous increase after yielding. The load of the specimens bonded with Silicon A increased rapidly immediately after loading. After the CFRP was peeled off from the column and sill, the 50S and 50P specimens showed no increase in load, whereas the 75P specimens exhibited an increase in load. The load of the Silicon B-bonded specimens increased to approximately 10 kN and then rapidly decreased owing to the peeling of the CFRP plate. Additionally, the Epoxy-bonded specimens exhibited a significant decrease in load owing to peeling of the CFRP plate. The shear strength of Epoxy was higher than that of Silicon B (Table 2). For the 50P and 75P specimens, the maximum loads of the Epoxy-bonded specimens were greater than those of the Silicon B-bonded specimens. However, for the 50S specimens, the maximum load of the Epoxy-bonded specimens was smaller than that of the Silicon B specimen. The surface roughness of the CFRP plate can vary among the plates owing to inconsistent sanding, and the difference in surface roughness can affect the maximum load of the 50S specimens.

The envelope load–displacement curves are shown for each failure mode. The specimens that showed failure by screw tear out, screw head pull-through, and split of the sill showed no difference in the shape of the load–displacement curves. The specimens that exhibited buckling of the CFRP plate showed a sudden and significant decrease in load owing to failure. The buckling failure of CFRP should be avoided because of the possible sudden loss of resistance of the column–sill joint owing to the cyclic load. A 0.75 mm CFRP plate would be preferable over a 0.50 mm one to avoid buckling failure.

3.3 Strength Properties

The initial stiffness and maximum load of the column–sill joint specimens were obtained from the envelope load–displacement curves. The line calculated by the least squares method using load and displacement data from the origin to 50% of the maximum load was defined as the initial stiffness.

The initial stiffness and maximum load of the column–sill joint specimens are shown in Fig. 11. The specimens with bonds exhibited a higher initial stiffness than did those without bonds. The initial stiffness of the 50S specimens increased with the increasing shear strength of the bond. The initial stiffness was higher for the 50P and 75P Silicon B specimens than that for the 50P and 75P Silicon A and Epoxy specimens. This was because of the method used to evaluate the initial stiffness. The loads of the 50P and 75P Silicon B- and Epoxy-bonded specimens first increased linearly (Fig. 10), and the slope of the increase changed at approximately 5 kN. The slope after 5 kN was less steep for the Epoxy-bonded specimens than for the Silicon B-bonded specimens. Because the data up to 50% of the maximum load were used for the calculation of initial stiffness, the initial stiffness of the Epoxy-bonded specimens would be determined as low. For the Silicon B- and Epoxy-bonded specimens, the secant stiffness, the slope of the line passing through the origin and a point on the curve corresponding to 5 kN, was calculated.

The mean secant stiffness values of the 50S Silicon B- and Epoxy-bonded specimens were 7.97 and 9.24 kN/mm, those of the 50P Silicon B- and Epoxy-bonded specimens were 7.43 and 6.49 kN/mm, and those of the 75P Silicon B- and Epoxy-bonded specimens were 7.03 and 6.83 kN/mm, respectively. For the 50P and 75P specimens, the secant stiffness showed a similar value, irrespective of the type of bond. For a CFRP plate that excluded the peel ply with a shear strength of the bond > 5.62 MPa, the load–displacement behavior during a small displacement of the column–sill joint showed similar values.
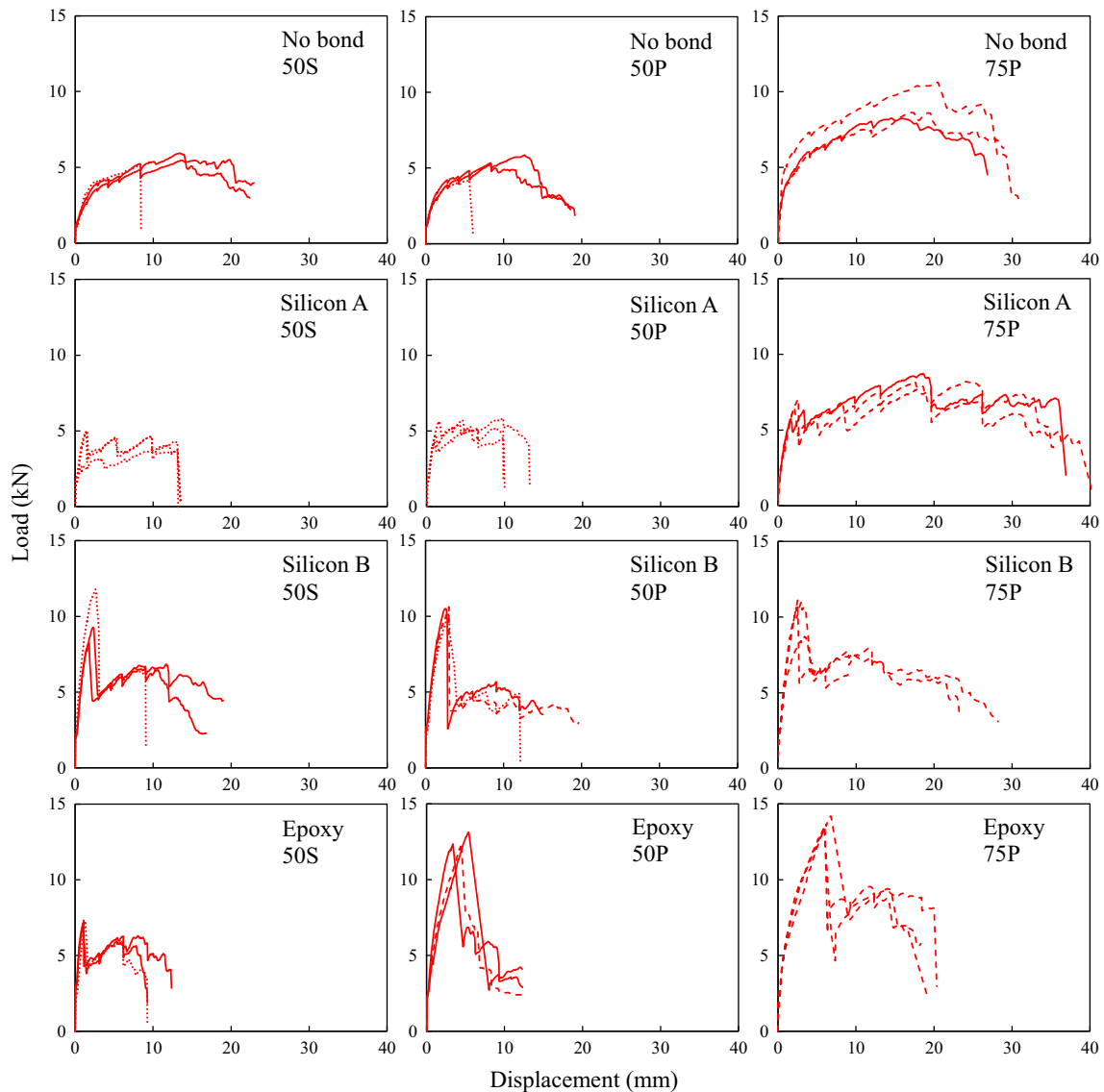
Fig. 10 Relationship between load and displacement: Solid line, tear out and screw head pull-through; broken line, split of sill; dotted line, buckling of CFRP plate

For the 50S Silicon A-bonded specimens, the maximum load was similar to that of the no-bond specimens and reflected the lowest values (Fig. 11b). The maximum load of the 50S Epoxy-bonded specimens was lower than that of the Silicon B-bonded specimens. As the shear strength of Epoxy was higher than that of Silicon B, the bonding performance of Epoxy-bonded specimens was not fully reflected in the maximum load of the specimens. The sanding of the CFRP plate may not have created sufficient surface roughness.

The maximum load of the 50P and 75P Silicon A-bonded specimens was comparable to that of the no-bond specimens, and the maximum load of the specimens increased as the shear strength of the bond increased. The maximum loads of the 75P specimens were generally higher than those of the 50P specimens for the no-bond and Silicon A-bonded specimens; the maximum loads for the Silicon B- and Epoxy-bonded specimens were very similar to those of the 50P specimens. This shows that the thickness of the CFRP plate influenced the maximum load of the no-bond and Silicon A-bonded specimens but had little effect on the Silicon B- and Epoxy-bonded specimens.

3.4 Load–Displacement Behavior After Peeling of CFRP Plate

Schematic diagrams of the load–displacement curves of the column–sill joints with and without bonds are shown in Fig. 12. The column–sill joint with a bond resisted the uplift force by the shear resistances of the bonded and
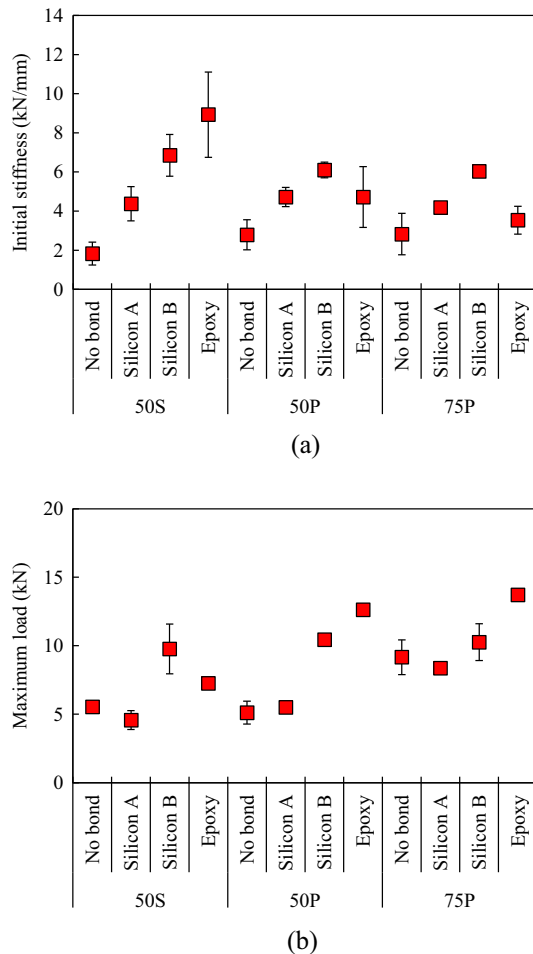
Fig. 11 Initial stiffness and maximum load of column–sill joint specimens: **a** initial stiffness; **b** maximum load. Bars indicate standard deviation

Fig. 12 Model of load–displacement curve: **a** column–sill joint specimen without bonds; **b** column–sill joint specimen with bonds

Fig. 13 Maximum load after peeling bonded specimens divided by maximum load of no-bond specimens. Bars indicate standard deviation

screwed joints. When the displacement of the column–sill joint was small, as shown in image I in Fig. 12, most of the resistance of the column–sill joint was attributed to that of the bonded joint. When the bonded joint failed and the CFRP plate peeled off, the screwed joints resisted the uplift force. The load–displacement behavior of the column–sill joint specimens with bonds after CFRP peeling (image II in Fig. 12) was compared with that of the no-bond specimens. The maximum load (P_{S-max}) and displacement corresponding to 80% of the maximum load ($0.8 \times P_{S-max}$) over the maximum load were determined for the no-bond specimens. For the bonded specimens, the maximum load (P_r) after peeling the CFRP plate and the displacement corresponding to the value of $0.8 \times P_{S-max}$, obtained from the no-bond specimens, were determined.

The value of P_r was divided by the mean value of the maximum load of the column–sill joint no-bond specimens, and the results were expressed in terms of P_r/P_{S-max}, as shown in Fig. 13. The P_r/P_{S-max} value did not change
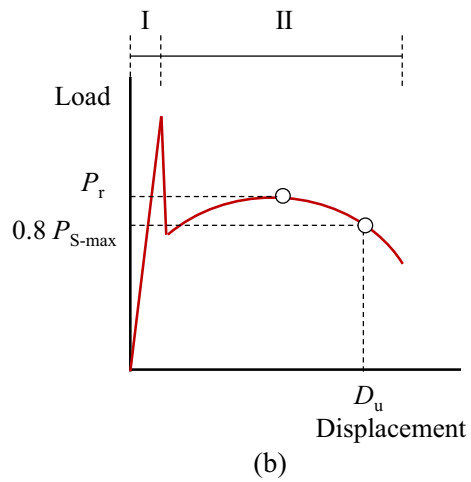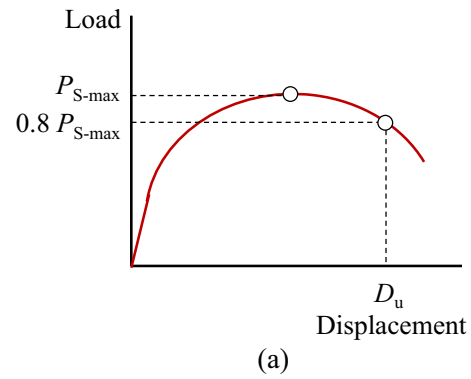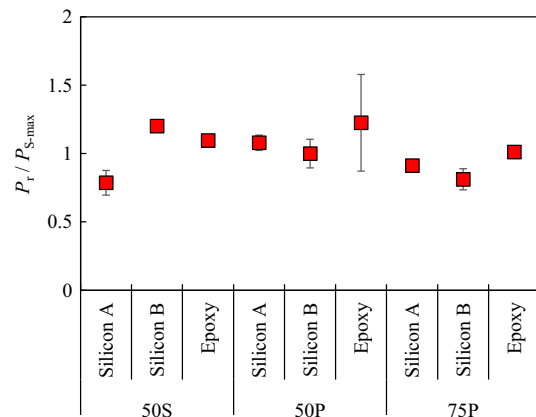
significantly, irrespective of the CFRP plate or bond composition, and the average remained in the range of 0.79–1.23. After peeling the CFRP plate, the bonded specimens exhibited resistance similar to that of the no-bond specimens.
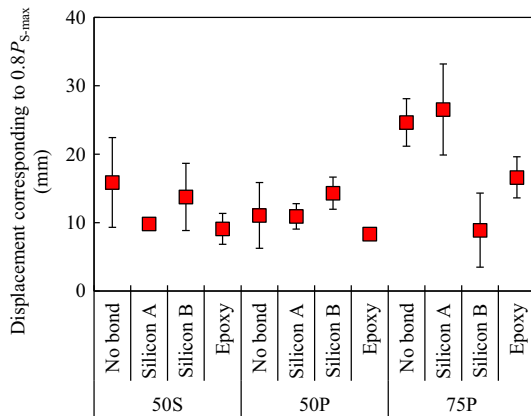
Fig. 14 Displacement at 80% of maximum load. Bars indicate standard deviation

The displacement (D_u) corresponding to a value of $0.8 \times P_{S\text{-max}}$ is shown in Fig. 14. The column–sill joint 50S and 50P specimens showed no clear difference between the values of D_u of the specimens with and without bonds. However, the values of D_u of the 75P specimens depended on the bond type. The values of D_u of the Silicon A specimens were similar to those of the no-bond specimens, and the Silicon B and Epoxy specimens exhibited significantly smaller values. When a bond with high shear strength is used in a column–sill joint with a CFRP plate, a significant decrease in load owing to the peeling of the CFRP plate can influence the deformation performance of the screwed joints.

When the CFRP plate is installed in the column–sill joint with both a bond and screws, the plate with the peel ply is recommended over that with sanding because sanding can cause variations in the consistency of the finish when creating surface roughness. The preferred thickness of the CFRP plate is 0.75 mm because the 0.50-mm thick CFRP plates under cyclic loading can fail due to buckling, which causes a rapid decrease in the load. When a high shear strength bond is used, the column–sill joint shows high resistance during small displacements and high maximum loads, although the deformation performance after peeling the CFRP plate can be lower.

4 Conclusions

Cyclic loading tests were conducted on column–sill joints with CFRP plates installed with bonds and screws. A total of 12 specifications comprising different combinations of CFRP plate surface finishes, thicknesses, and types of bonds were evaluated. The results are summarized as follows:

1. The failure of the column–sill joint specimens exhibited the following three modes: screw tear out and screw head pull-through in the CFRP plate, splitting of the sill, and buckling of the CFRP plate, in addition to peeling of the CFRP plate. The 0.50 mm thick CFRP plate specimens exhibited all three failure modes. The 0.75 mm thick CFRP plate specimens showed failure in the screw tear out and screw head pull-through in the CFRP plate and split of the sill, but did not fail owing to buckling of the CFRP plate.

2. The specimens that failed with screw tear out and screw head pull-through or split of the sill showed no difference in the shape of the load–displacement curves. The specimens that failed owing to buckling of the CFRP plate showed a rapid and significant decrease in load.

3. The initial stiffness of the column–sill joint specimens tended to increase with the bond shear strength. Although the stiffnesses of the 50P and 75P CFRP plate Epoxy-bonded specimens were lower than those of the specimens bonded with Silicon B, the cause of this is considered the evaluation method of the initial stiffness; little difference in the secant stiffness values was observed.

4. The maximum load of the column–sill joint specimens increased with the shear strength of the bond, except for the 50S specimens, in which sanding created insufficient surface roughness. The 75P specimens showed a larger maximum load than the 50P Silicon A-bonded specimens and a similar maximum load to the 50P Silicon B- and Epoxy-bonded specimens.

5. The maximum load of column–sill joint specimens after peeling of the CFRP plate was similar to the maximum load of the no-bond specimens.

6. The maximum load of the 75P CFRP plate Silicon B- and Epoxy-bonded specimens improved, and the load after peeling of the CFRP plate decreased faster.

Springer

Declarations

Conflict of interest The authors declare that they have no conflict of interest.

Open Access This article is licensed under a Creative Commons Attribution 4.0 International License, which permits use, sharing, adaptation, distribution and reproduction in any medium or format, as long as you give appropriate credit to the original author(s) and the source, provide a link to the Creative Commons licence, and indicate if changes were made. The images or other third party material in this article are included in the article's Creative Commons licence, unless indicated otherwise in a credit line to the material. If material is not included in the article's Creative Commons licence and your intended use is not permitted by statutory regulation or exceeds the permitted use, you will need to obtain permission directly from the copyright holder. To view a copy of this licence, visit http://creativecommons.org/licenses/by/4.0/.

References

1. Japan Building Disaster Prevention Association (2011) Revision for 2010 Guide for design and construction of aseismic retrofitting of existing reinforced concrete construction utilizing continuous carbon fiber reinforcement material (**in Japanese**)
2. American Concrete Institute (2008) Guide for design and construction of externally bonded frp systems for strengthening concrete structures
3. Consiglio Nazionale delle Ricerche (2006) Guide for the design and construction of externally bonded FRP systems for strengthening existing structures
4. Cao S, Chen J, Pan J, Sun N (2007) ESPI measurement of bond–slip relationships of FRP–concrete interface. J Compos Constr 11(2):149–160
5. Mazzotti C, Savoia M, Ferracuti B (2008) An experimental study on delamination of FRP plates bonded to concrete. Constr Build Mater 22(7):1409–1421
6. Nakaba K, Kanakubo T, Furuta T, Yoshizawa H (2001) Bond behavior between fiber–reinforced polymer laminates and concrete. ACI Struct J 98(3):359–367
7. Dai J, Ueda T, Sato Y (2006) Unified analytical approaches for determining shear bond characteristics of FRP–concrete interfaces through pullout tests. J Adv Concr Technol 4(1):133–145
8. Ferracuti B, Savoia M, Mazzotti C (2007) Interface law for FRP–concrete delamination. Compos Struct 80(4):523–531
9. Vahedian A, Shrestha R, Crews K (2018) Analysis of externally bonded carbon fibre reinforced polymers sheet to timber interface. Compos Struct 191:239–250
10. Biscala HC, Diogo P (2020) Experimental analysis of different anchorage solutions for laminated carbon fiber–reinforced polymers adhesively bonded to timber. Compos Struct 243:112228
11. Consiglio Nazionale delle Ricerche (2007) Guide for the design and construction of externally bonded FRP systems for strengthening existing structures – Timber structures
12. Wan J, Smith ST, Qiao P, Chen F (2014) Experimental investigation on FRP-to-timber bonded interfaces. J Compos Constr 18(3):A4013006
13. Corradi M, Righetti I, Borri A (2015) Bond strength of composite CFRP reinforcing bars in timber. Materials 8(7):4034–4049
14. Biscala HC, Cruz D, Chastre C (2016) Analysis of the debonding process of CFRP-to-timber interfaces. Constr Build Mater 113:96–112
15. Biscala H, Chastre C, Cruz D, Viegas A (2017) Prediction of the interfacial performance of CFRP laminates and old timber bonded joints with different strengthening techniques. Compos B Eng 108:1–17
16. Vahedian A, Shrestha R, Crews K (2017) Effective bond length and bond behaviour of FRP externally bonded to timber. Constr Build Mater 151:742–754
17. Vahedian A, Shrestha R, Crews K (2018) Bond strength model for externally bonded FRP–to–timber interface. Compos Struct 200:328–329
18. Schober KU, Rautenstrauch K (2006) Post–strengthening of timber structures with CFRP's. Mater Struct 40:27–35
19. Garcia PR, Escamilla AC, Garcia MNG (2013) Bending reinforcement of timber beams with composite carbon fiber and basalt fiber materials. Compos Part B 55:528–536
20. Khelifa M, Lahouar MA, Celzard A (2015) Flexural strengthening of finger-jointed Spruce timber beams with CFRP. J Adhes Sci Technol 29(19):2104–2116
21. Schober KU, Harte AM, Kliger R, Jockwer R, Xu Q, Chen JF (2015) FRP reinforcement of timber structures. Constr Build Mater 97:106–118
22. Biscala HC, Chastre C, Cruz D, Franco N (2017) Flexural strengthening of old timber floors with laminated carbon fiber–reinforced polymers. J Compos Constr 21(1):04016073
23. Rescalvo FJ, Valverde-Palacios I, Suarez E, Gallego A (2018) Experimental and analytical analysis for bending load capacity of old timber beams with defects when reinforced with carbon fiber strips. Compos Struct 186:29–38
24. Righetti L, Corradi M, Borri A (2015) Strengthening of timber beams with unbonded FRP composites. In: 16th European Bridge Conference, 23–25 June 2015, Edinburgh
25. Righetti L, Corradi M, Borri A (2016) Shear resistance of screwed timber connections with parallel to grain FRP reinforcements. WCTE2016, Vienna
26. Kanerva M, Saarela O (2013) The peel ply surface treatment for adhesive bonding of composites: a review. Int J Adhes 43:60–69
27. Buchman C, Langer S, Filsinger J, Drechsler K (2016) Analysis of the removal of peel ply from CFRP surfaces. Compos Part B 89:352–361
28. Japan Housing and Wood Technology Center (2017) Allowable stress calculation of conventional post and beam housing 1. pp 300–311 (**in Japanese**)